第 43 卷第 1 期
2024 年 2 月

红 外 与 毫 米 波 学 报
J. Infrared Millim. Waves

Vol. 43, No. 1
February, 2024

文章编号：1001-9014(2024)01-0052-11

DOI:10. 11972/j. issn. 1001-9014. 2024. 01. 008

Recent advances in on-chip infrared polarization detection

ZHEN Yu-Ran[1,2], DENG Jie[1*], BU Yong-Hao[1,2], DAI Xu[1,2], YU Yu[1,2], SHI Meng-Die[1,2], WANG Ruo-Wen[1,2], YE Tao[1,2], CHEN Gang[1,2*], ZHOU Jing[1,2*]

(1. State Key Laboratory of Infrared Physics, Shanghai Institute of Technical Physics, Chinese Academy of Sciences, Shanghai 200083, China;
2. University of Chinese Academy of Sciences, Beijing 100049, China)

Abstract: Polarization is an intrinsic degree of freedom of light. The detection of polarization light provides more information in addition to light intensity and wavelength. Infrared polarization detectors play a vital role in numerous applications, such as imaging, communication, remote sensing, and cosmology. However, traditional polarization detection systems are bulky and complex, hindering the miniaturization and integration of polarization detection. Recently, the development of on-chip infrared polarization detectors has become an area of great interest. In this review, we focus on two recent advanced research areas of on-chip infrared polarization detectors: polarization-sensitive materials and integration of polarization-selective optical coupling structures. We discuss the current research status, future challenges and opportunities for the development of on-chip infrared polarization detectors.

Key words: infrared polarization detector, anisotropic materials, topological materials, chiral perovskites, polarization-selective optical coupling structures

片上红外偏振探测研究进展

甄玉冉[1,2], 邓 杰[1*], 布勇浩[1,2], 代 旭[1,2], 余 宇[1,2], 石梦碟[1,2], 王若文[1,2], 叶 韬[1,2], 陈 刚[1,2*], 周 靖[1,2*]

(1. 中国科学院上海技术物理研究所 红外物理国家重点实验室,上海 200083;
2. 中国科学院大学,北京 100049)

摘要:偏振是光的固有自由度,偏振探测提供了光强和波长之外的更多丰富信息。红外偏振探测器在成像、通信、遥感和宇宙学等众多应用中发挥着至关重要的作用。然而,传统的偏振检测系统体积庞大、系统复杂,阻碍了偏振探测的小型化和集成化。近来,片上红外偏振探测器的发展引起了广泛的研究兴趣。本文将重点介绍片上红外偏振探测器的两个前沿研究领域:偏振敏感材料和偏振选择性光耦合结构集成的红外偏振探测器,主要讨论片上红外偏振探测器的研究现状以及未来的挑战和机遇。

关 键 词:红外偏振探测器;各向异性材料;拓扑材料;手性钙钛矿;偏振选择性光学耦合结构

中图分类号:O43; **文献标识码**:A

Introduction

Infrared polarization detection has numerous important applications, including military reconnaissance, quantum communication, cosmology, biomedicine, and remote sensing[1]. However, traditional polarization detection systems are bulky and complex, hindering the

Received date: 2023-04-24, **revised date**: 2023-06-24 **收稿日期**:2023-04-24,**修回日期**:2023-06-24

Foundation items: Supported by the National Key Research and Development Program of China (2022YFA1404602), the Strategic Priority Research Program of the Chinese Academy of Sciences (Grant No. XDB0580000), the National Natural Science Foundation of China (61975223, 61991442, 62305362, 62075230), the Key Deployment Projects of the Chinese Academy of Sciences (ZDRW-XH-2021-7-1), the Program of Shanghai Academic/Technology Research Leader (22XD1424400), the Shanghai Municipal Science and Technology Major Project (2019SHZDZX01), Natural Science Foundation of Shanghai (19ZR1465400).

Biography: ZHEN Yu-Ran (1997-), female, Hebei, master. Research area involves Infrared polarization detection materials and devices. E-mail: 1961213356@qq. com.

* **Corresponding author**: E-mail: dengjie@mail. sitp. ac. cn, gchen@mail. sitp. ac. cn, jzhou@mail. sitp. ac. cn

miniaturization and integration of polarization detection. On-chip infrared polarization detectors with the advantages of small size, high responsivity, and high polarization extinction ratio, represent the future of polarization detection[2]. To realize advanced infrared polarization detectors, we primarily focus on enhancing polarization discrimination and miniaturizing device sizes.

The polarization-sensitive materials offer a straightforward way to realize polarization detection. Polarization detectors based on anisotropic materials have compact structures and require no extra fabrication processes compared to common detectors[3-11]. Recently, a lot of anisotropic or chiral materials have been proposed for polarization detection. Anisotropic van der Waals materials and heterostructures are studied for linear polarization detection[12-21]. Chiral hybrid perovskites, topological materials, and other circular-polarization-sensitive materials are demonstrated to be able to distinguish the handedness of circularly polarized light[22-24]. Although the polarization detectors based on polarization-sensitive materials can realize either linear or circular polarization detection, the choice of these materials is quite limited. In addition, poor chemical stability, low responsivity, and low polarization extinction ratio also hinder the development of detectors based on polarization-sensitive materials.

Thanks to advances in micro- and nano-fabrication techniques, polarization-selective optical coupling structures have been successfully integrated with infrared materials to enhance the performance of polarization detectors[24-28]. By combining the advantages of polarization-selective optical coupling structures and the anisotropic absorption in materials, the integration of polarization-selective plasmonic microcavities and anisotropic materials exhibits a double enhancement of polarization discrimination[25]. Recently, configurable photocurrent polarity has also been achieved by manipulating local photocurrent density through plasmonic nanoantennas. The polarity of photocurrent is tunable by light polarization flexibly and an infinite extinction ratio could be realized at the polarity-transition point.

In this review, we will introduce the infrared polarization detectors based on polarization-sensitive materials in Section 1. Then the integration of polarization-selective optical coupling structures will be discussed as follows in Section 2. At last, in Section 3, we talk about the next challenge and opportunity for the detection of full Stokes parameters in the future.

1 Polarization-sensitive materials

Traditional methods of linear or circular polarization detection involve rotating polarizers or waveplates. Most detection materials are polarization-insensitive and can only detect light intensity. The requirement of numerous discrete optical components in traditional polarization detection systems hinders the miniaturization and integration of polarization detection systems. Polarization-sensitive materials have been widely investigated to construct compact and filterless polarization detectors.

1.1 Anisotropic absorption in two-dimensional materials

Two-dimensional materials have been extensively studied in the field of optoelectronics due to their unique optical and electronic properties. Anisotropic absorption in some two-dimensional materials promises sensitivity to linearly polarized light[2]. These materials offer a straightforward approach to on-chip infrared polarization detectors and demonstrate excellent performance. The polarization detection systems consisting of anisotropic two-dimensional materials have the advantage of miniaturization compared to traditional methods.

In 2020, Lei Tong et al. utilized high-mobility, narrow-bandgap, anisotropic quasi-two-dimensional tellurium (Te) photodetectors to achieve target imaging with a linear polarization extinction ratio greater than 9 at the wavelength of 2.3 μm[29]. Fig. 1 (a) shows the schematic device structure and the polarization-dependent photoresponse. The polarization detection based on individual anisotropic materials is very compact. The characteristics of the polarization detector, including linear polarization extinction ratio and response wavelength, rely on the anisotropic absorption of the material.

In 2022, Wenjie Deng et al. constructed a twisted unipolar barrier van der Waals heterostructure using the anisotropic material b-AsP[30]. The heterostructure consisted of a b-AsP/WS_2/b-AsP configuration, forming a small barrier for electrons and a high barrier for holes to create a unipolar barrier by band engineering. The bias-switchable photocurrents are dominated by the anisotropic absorption at the top and bottom, respectively. The device realizes full polarization state detection of linearly polarized incident light in the mid-infrared band. The linear polarization extinction ratio is 55 under the bias of 0.1 V. Fig. 1 (b) shows the structure diagram of the heterojunction device and the polarization photocurrent under the external bias. Anisotropic two-dimensional materials are commonly used for linear polarization detection, and heterojunctions can be constructed based on these materials to enhance their anisotropic absorption through band engineering. However, achieving circular polarization detection using two-dimensional materials is challenging.

In 2021, Fang et al. demonstrated the use of inherent in-plane and out-of-plane optical anisotropy of MoS_2 to fabricate a full-Stokes polarimeter on a single-layer MoS_2/few-layer MoS_2 homojunction chip. This homojunction on-chip full-Stokes polarimeter is based on valley-dependent optical selection rules in monolayer MoS_2, which induces valley-locked spin-polarized photocurrent known as the circular photogalvanic effect (CPGE). The response is further enhanced by the monolayer MoS_2/few-layer MoS_2 homojunction, enabling the detection of all four Stokes parameters of incident light at zero bias in the 650 ~ 690 nm wavelength range[31]. Fang et al. employed mechanical rotation to achieve an oblique incidence of light on the surface of an isotropic single-layer MoS_2/few-layer MoS_2 homojunction. Fig. 1 (c) shows the schematic diagram of the homojunction device test and

the photocurrent as the function of the angle of the quarter-wave plate.

In 2022, Ma et al. achieved a breakthrough in realizing a tunable mid-infrared bulk photovoltaic effect by utilizing twisted double bilayer graphene (TDBG) at 5 μm and 7.7 μm wavelengths[32]. The TDBG device benefits from the strong symmetry-breaking properties of the graphene moiré superlattice material, as well as the nonlinear light-matter interaction regulated by quantum geometry. Additionally, the advanced machine learning algorithm, such as a convolutional neural network (CNN), is applied to recognize the double-gate-dependent bulk photovoltaic voltage mapping and achieve the full Stokes polarization reconstruction[32].

1.2 Linear and circular photogalvanic effect in topology materials

Topological materials exhibit novel optoelectronic phenomena due to their unique electronic band structure, involving the Berry curvature of the electron wavefunction[32]. Topological materials generate prominent photocurrent under linear and/or circular polarized light with broken inversion symmetry or time-reversal symmetry. These phenomena are known as the linear photogalvanic effect (LPGE) and circular photogalvanic effect (CPGE), respectively. Besides, topological semimetals hold promise for broadband infrared detection due to their gapless band structure at the Weyl point.

In 2018, Xu et al. demonstrated the tunable Berry curvature dipole of single-layer topological insulator WTe_2 to realize observable and electrically switchable CPGE[33]. The low-energy band structure of monolayer WTe_2 without spin-orbit coupling features tilted two-dimensional Dirac fermions at the Q and Q' points. The CPGE is induced by interband transitions of the inverted quantum spin Hall (QSH) gap near the Q and Q' points located close to the bottom of the conduction band. The inverted band structure and tilted crystal lattice of monolayer WTe_2 produce Berry curvature dipoles and strong electric field effects, resulting in an observable and electrically switchable CPGE for circularly polarized light detection.

In 2018, Lai et al. developed a self-powered photodetector with broadband capabilities, utilizing a type-II Weyl semimetal T_d-$MoTe_2$. The anisotropy of this material is wavelength-dependent, with greater anisotropy at excitation wavelengths closer to the Weyl node. T_d-$MoTe_2$ is a promising material for broadband polarization-sensitive and self-powered photodetection with excellent response. Based on the anisotropy of T_d-$MoTe_2$, there are anisotropic photocurrent responses at different linear polarization excitation of 10.6 μm, 4 μm, and 633 nm, and the linear polarization extinction ratios are 2.72, 1.92 and 1.19, respectively[22]. Afterward in 2022, Ma et al. conducted a study on the semiconductor material Te. They discovered that under 10.6 μm and 4.0 μm photoexcitation, the material exhibited opposite CPGE directions due to the chirality-dependent optical selection rules for transitions between the valence band and the conduction band of the semiconductor material Te between Weyl cones[23].

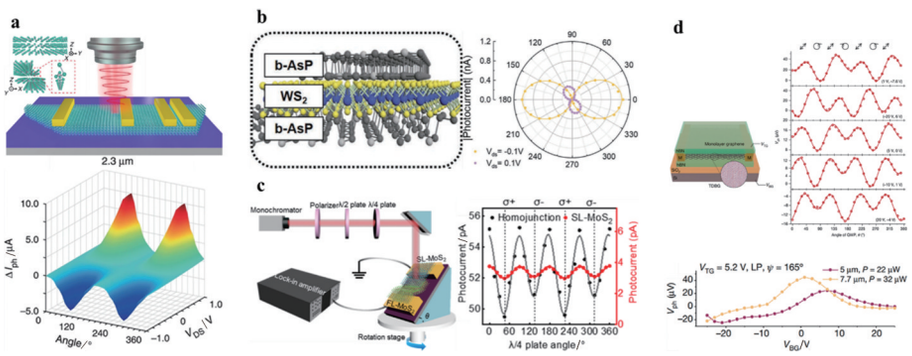

Fig. 1 (a) Schematic diagram of tellurium (Te) crystal structure. Schematic diagram of the device structure. At room temperature, the incident power is 6.0 mW, and the net polarized photocurrent ΔI_{ph} is when the incident wavelength is 2.3 μm[29]; (b) Schematic diagram of the unipolar barrier van der Waals heterostructure photodetector composed of b-AsP/WS_2/b-AsP. Polar plots of linear polarization angle-dependent forward-bias-driven photocurrent and reverse-bias-driven photocurrent[30]; (c) Schematic diagram of the full-Stokes polarization measurement setup. Comparison of helicity-dependent photocurrents at 0 V and -0.1 V for homostructure devices and monolayer MoS_2 [31]; (d) Schematic of a twisted double bilayer graphene (TDBG) photodetector. Photovoltage (V_{ph}) as a function of the quarter-wave plate (QWP) angle (θ) at different gate voltage biases (V_{BG}, V_{TG}) measured at T = 79 K and λ = 5 μm. Photovoltage function of V_{BG} excited by 5 μm and 7.7 μm linearly polarized light (LP) when ψ = 165° and V_{TG} = 5.2 V[32]

图1 (a) Te的晶体结构和器件结构示意图,在入射功率为6.0 mW,入射波长为2.3 μm时,室温下的净偏振光电流ΔI_{ph}[29],(b) 由b-AsP/WS_2/b-AsP构成的单极势垒范德瓦尔斯异质结光电探测器的示意图,线偏振角依赖的正向偏置和反向偏置光电流[30],(c) 全斯托克斯偏振测量的示意图,单层-少层MoS_2同质结器件和单层MoS_2器件在0 V和-0.1 V时的螺旋度依赖的光电流的对比[31],(d) 扭曲双层石墨烯光电探测器的示意图,温度为79 K,入射波长为5 μm时,测量不同顶栅和背栅栅压(V_{BG},V_{TG})下,四分之一波片角度依赖的光电压,当线偏振角为165°,顶栅栅压为5.2 V,入射波长5 μm和7.7 μm的线偏光激发时,不同背栅栅压下的光电压[32]

In 2019, Osterhoudt et al. employed the topological structure of Weyl semimetal TaAs and focused ion beam (FIB) manufacturing technology to achieve the giant bulk photovoltaic effect (BPVE) in the 10.6 μm band at room temperature[34]. The investigation of the nonlinear optical properties of TaAs revealed that the CPGE is related to electronic chirality in TaAs.

1.3 Chiral perovskite and organic materials

Chiral materials are defined as objects that cannot be superimposed on their mirror images. Due to their distinct chiral properties, they find diverse applications in fields such as medicine, biology, and quantum technology[35]. The differential absorption of left-handed circularly polarized light (LCP) and right-handed circularly polarized light (RCP) by chiral perovskite and organic materials offers the opportunity to directly detect circularly polarized light (CPL).

In 2019, Chen et al. fabricated a CPL detector using chiral organic-inorganic hybrid (α -PEA) PbI_3 perovskite. To synthesize the chiral perovskite, they selected chiral α-phenylethylamine, whose π bond on the benzene ring aids in the positional interaction between the chiral amine and the $(PbI_6)^{4-}$ matrix, enhancing the CPL-sensitive absorption. The circularly polarized detector exhibited a maximum polarization extinction ratio of 1.1 around the wavelength of 395 nm, a responsivity of 797 mA/W^{-1}, and a detectivity of 7.1×10^{11} Jones[36]. The device remained stable for one month. Although direct detection of CPL was achieved, the circular polarization extinction ratio (CPER) is not sufficient.

In 2020, Ishii et al. fabricated a CPL detector using the helical one-dimensional (1D) structure of lead halide perovskite, which is composed of naphthyl ethylamine-based chiral organic cations[37]. The 1D structure consists of face-sharing $(PbI_6)^{4-}$ octahedral chains, and R-(+)- and S-(−)-1-(1-naphthyl) ethylamine were chosen as the chiral cations in the 1D perovskites. The helicity of the 1D structure is primarily influenced by the chiral cations, resulting in an extremely high CPER. This work reported the highest CPER (25.4 at the wavelength of 395 nm) of perovskite based circular polarization detectors.

In 2021, Liu et al. incorporated chiral organic ligands into the inorganic octahedral framework $(PbX_6)^{4-}$ of perovskite to create an optically active chiral hybrid perovskite (CHP) with efficient charge transport[38]. The chiral ligand has a large π bond on the benzene ring, facilitating the Coulomb interaction between the chiral amine and the $(PbI_6)^{4-}$ matrix, which enhances CPL-sensitive absorption. They fabricated CPL detectors with high photocurrent and polarization selectivity using CHP single-crystal nanowire arrays. The CPL detectors exhibited a CPER of 1.27, an on-off ratio of 1.8×10^4, and a responsivity of 1.4 A/W^{-1} at 510 nm with a bias voltage of 5 V.

In 2022, Cao et al. created a new van der Waals heterojunction by combining a two-dimensional chiral hybrid perovskite material $(MBA)_2PbI_4$ with black phosphorus (BP)[39]. The interfacing perovskite provides an inflow of numerous photogenerated carriers to BP, to reinforce the charge carrier transfer, separation, and transport processes. The responsivity and photogain of BP in heterostructures are boosted by almost one order of magnitude with respect to BP alone, which is more obvious under excitation above the bandgap of perovskite. The linear polarized light extinction ratio of the van der Waals heterojunction reaches 9 at a wavelength of 1 550 nm.

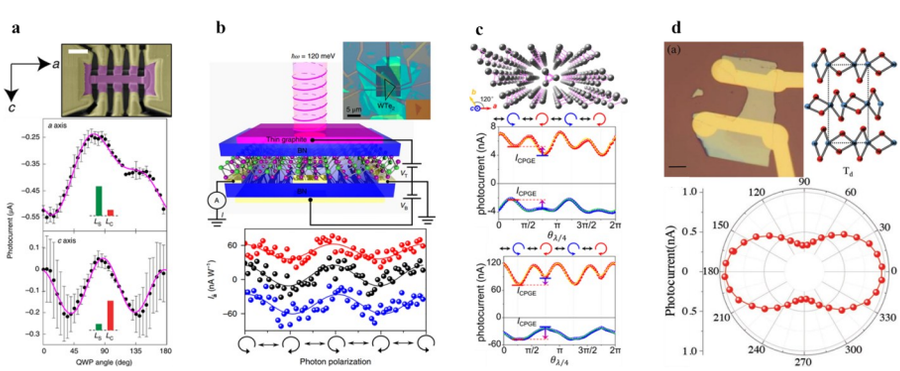

Fig. 2 (a) False-color scanning electron microscope image of a TaAs device. Along the *a*-axis and *c*-axis, the photocurrent varies with the angle of the quarter-wave plate[34]; (b) Schematic experimental set-up for detecting the mid-infrared circular photogalvanic effect on a dual-gated monolayer WTe_2 device. Polarization along the *a*-axis depends on the photocurrent[33]; (c) The lattice structure of tellurium (Te). The quarter-wave plate-dependent photocurrent at the position of the maximum positive and negative response of the Te device under 10.6 μm (middle) and 4 μm (bottom) excitation[23]; (d) Optical microscope image of the $MoTe_2$ device. Crystal structure of T_d-$MoTe_2$. Anisotropic photocurrent response with a polarization extinction ratio of 2.72 for linearly polarized excitation at 10.6 μm[22]

图2 (a) TaAs器件的伪彩色扫描电子显微镜图像,沿*a*轴和*c*轴的随四分之一波片角度变化的光电流[34],(b) 双栅调控单层WTe_2器件的中红外圆偏光电流测试的示意图,沿*a*轴的偏振依赖光电流[33],(c) Te的晶格结构,在激发波长为10.6 μm(中)和4 μm(下)时,Te最大正、负响应位置的四分之一波片角度依赖的光电流[23],(d) $MoTe_2$器件的光学显微镜照片,T_d相$MoTe_2$的晶体结构,激发波长为10.6 μm时,各向异性光电流响应的线偏振消光比达到2.72[22]

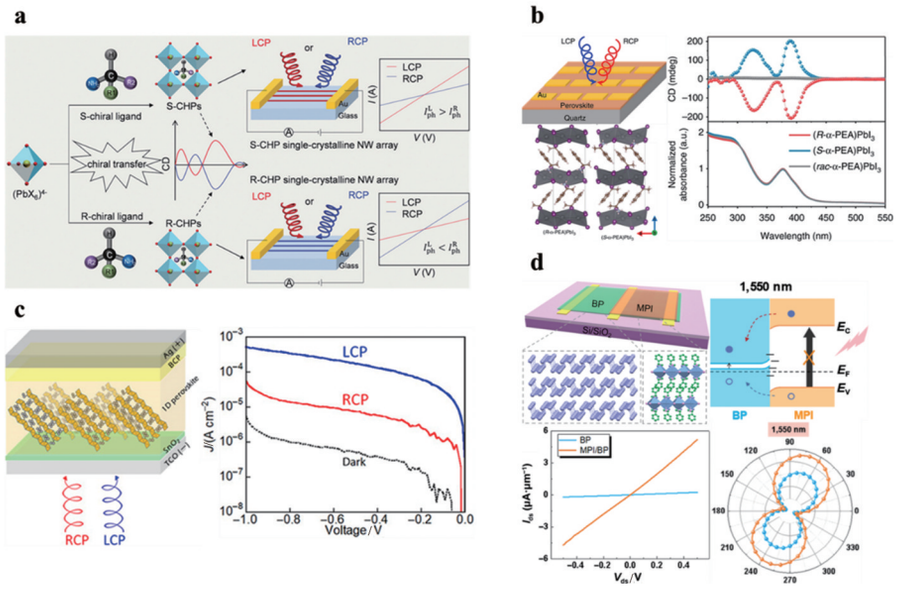

Fig. 3 (a) Chiral hybrid perovskite (CHP) single-crystal array design for high-performance CPL direct photodetection[38]; (b) Schematic of the photodetector. Crystal structure of (R- and S-α-PEA) PbI_3. Circular dichroism (CD) and absorbance spectra of (R-, S-, and rac-α-PEA) PbI_3 thin films[36]; (c) Schematic diagram of a helical one-dimensional perovskite-based photodetector. J-V curves of (R-NEA) PbI_3 device under LCP and RCP with a wavelength of 395 nm and an intensity of 1.0 mW cm^{-2}[37]; (d) Schematic diagram and crystal structure of vdW heterostructure photodetector device based on BP and chiral perovskite MPI. Electron and hole transfer process of MPI/BP heterostructure under 1 550 nm illumination. Heterostructure output curves and individual BPs. Polar plot of the normalized polarization photocurrent measured at an illumination power of 100 μW and a wavelength of 1 550 nm[39]

图3 (a) 用于圆偏振光直接探测的手性杂化钙钛矿单晶阵列设计[38], (b) PbI_3光电探测器的示意图, (R- and S-α- PEA) PbI_3的晶体结构, (R-, S-, and rac-α- PEA) PbI_3薄膜的圆二色性和吸收光谱[36], (c) 螺旋一维钙钛矿基光电探测器示意图, (R-NEA) PbI_3器件在入射波长为395 nm, 光强为1.0 mW cm^{-2}时, 左旋圆偏振和右旋圆偏振的电流-电压曲线[37], (d) 基于BP和手性钙钛矿MPI的范德瓦尔斯异质结光电探测器的示意图及其晶体结构, MPI/BP异质结在1 550 nm光照下, 电子和空穴转移过程, MPI/BP异质结器件和单独BP器件的输出曲线, 及其在入射功率为100 μW, 入射波长为1 550 nm时, 归一化的偏振分辨光电流[39]

2 Integration of polarization-selective optical coupling structures

In the previous section, the detection of linearly and/or circularly polarized light is based on polarization-sensitive materials, such as anisotropic two-dimensional materials, topological materials, and chiral perovskites or organic materials. However, the choice of these materials is quite limited. Poor chemical stability, low responsivity, and low polarization extinction ratio are the main problems for polarization detectors based on polarization-sensitive materials. On the other hand, artificial micro-nano optical structures show great potential in controlling the interaction between polarized light and matter. The polarization detectors with polarization-selective optical coupling structures, as well as the integration with anisotropic materials, show better performance in responsivity and polarization extinction ratio.

2.1 Polarization-selective optical coupling structures

Plasmonic structures play an important role in the interaction between light and matter. They enhance the polarization-dependent optoelectronic coupling through resonant excitation of localized surface plasmons. Therefore, plasmonic structures are important tools for achieving polarization-selective coupling. Different resonances with the enhanced localized optical field can be realized under specific polarizations of the incident light and then the polarization light is discriminated. Integration of the polarization-selective optical coupling structures and infrared detection materials can greatly improve polarization detection performance.

In 2014, Li et al. introduced a new approach to creating a grating plasmonic microcavity quantum well infrared detector by combining a single quantum well with a grating plasmonic microcavity[40]. The quantum well is employed as the active structure within the near-field region of the plasmonic effect enhanced cavity, with the localized surface plasmon (LSP) mode and the surface plasmon polariton (SPP) mode being controlled. The artificial plasma modulation significantly influences the propagation and distribution of light within the plasma microcavity, resulting in a high infrared polarization resolution capability for the grating plasmonic microcavity quantum well infrared detection device. Moreover, the device achieves an extinction ratio of 65 at 14.7 μm.

In 2015, Li et al. utilized a periodic array of chiral metamolecules comprised of a 'Z'-shaped silver antenna

on a poly (methyl methacrylate) spacer and an optically thick silver backplane to create a chiral plasmonic nanostructure with hot electron injection[41]. Plasmonic nanostructures with engineered chirality can differentiate between left-handed circularly polarized (LCP) and right-handed circularly polarized (RCP) light, and photodetection is based on hot electron injection into silicon. The chiral plasmonic nanostructure circular polarization detector achieves a polarization extinction ratio of 3.4 at the wavelength of 1 340 nm.

In 2019, Wang et al. employed gold-coated helical carbon nanowire end-fired and dipolar aperture nanoantennas to fabricate circularly polarized photodetectors by rotating surface plasmons on the subwavelength scale and utilizing optical spin-orbit interactions[42]. The device allows for adjustable polarization control with a CPER of 64 at 1 550 nm, indicating that circularly polarized light can be locally achieved by applying the concept of a helical traveling wave antenna to a single plasmonic nanoantenna.

In 2020, Jiang et al. utilized an asymmetric n-shaped gold nanoantenna chiral plasmonic metasurface integrated with a single layer of $MoSe_2$ to create an ultrathin circular polarimeter[43]. The chiral plasmonic metasurface is utilized to selectively detect circularly polarized light, while the two-dimensional material determines the working wavelength range (visible to near-infrared). The circular polarization-dependent photocurrent response based on the left-handed and right-handed metasurfaces is verified. The ultra-thin circular polarimeter achieves an extinction ratio of 1.74 for the left-handed metasurface and 1.9 for the right-handed metasurface at the wavelength of 790 nm.

2.2　Integration of anisotropic material and polarization-selective optical coupling structures

Combining the advantages of polarization-selective optical coupling structures and the anisotropic absorption in materials, the integration of polarization-selective plasmonic cavities and anisotropic materials exhibits a double enhancement of polarization discrimination.

In 2018, Zhou et al. integrated an array of anisotropic plasmonic microcavity (PMC) with a quantum well

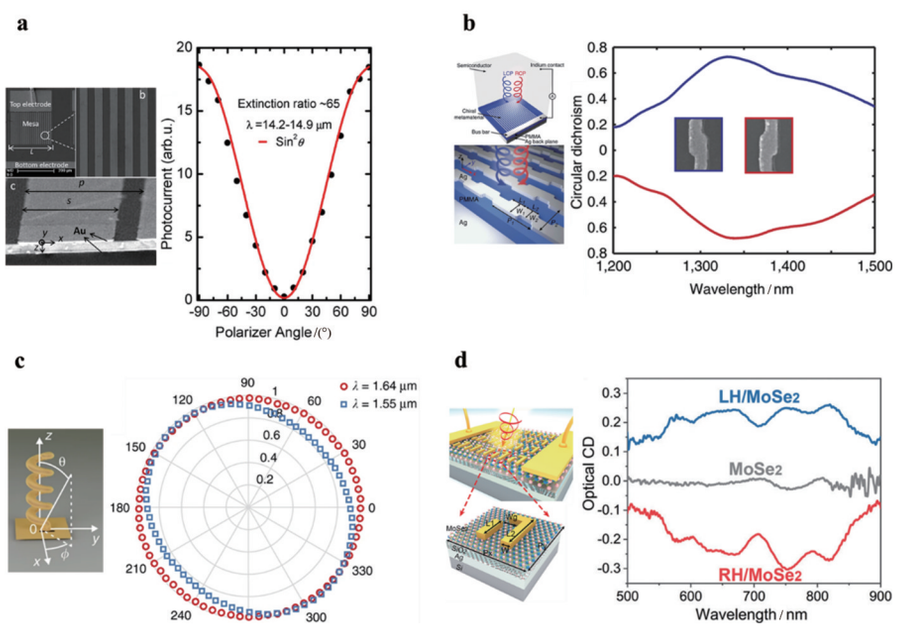

Fig. 4　(a) SEM image of the cleaved facet of the cavity structure. SEM image of PCQWID, a grating plasmonic microcavity quantum well infrared detector. The relationship between the average intensity of the photocurrent measured at the wavelength of 14.2 ~ 14.9 μm and the polarization angle of the incident light[40]; (b) Schematic of the chiral metamaterial and CPL detector. Experimentally measured circular dichroism spectra of the left-handed (LH, blue) and right-handed (RH, red) metamaterials[41]; (c) HTN schematic and how it works. The ellipticity factor of the output beam of the helical traveling wave nanoantenna HTN and the experimental spectrum of the DOCP. Polarization state analysis at wavelengths of 1.55 μm and 1.64 μm[42]; (d) Schematic illustration of the hybrid structure consisting of a chiral plasmonic metasurface and monolayer $MoSe_2$. Optical absorption spectra of left-handed and right-handed plasmonic metasurfaces illuminated by light[43]

图4　(a) 光栅等离激元微腔集成的量子阱红外探测器,微腔结构截面以及量子阱红外探测器的扫描电子显微镜图像,入射波长为14.2 ~ 14.9 μm时,随入射光偏振角变化的光电流平均强度[40], (b) 手性超材料及圆偏光探测器的示意图,实测的超材料圆二色光谱,左手性超材料(蓝色)和右手性超材料(红色)[41], (c) 螺旋行波纳米天线的示意图及其工作原理,螺旋行波纳米天线输出光束的椭圆率系数和圆偏振消光比的实验光谱,入射波长为1.55 μm和1.64 μm时的偏振态分析[42], (d) 单层$MoSe_2$和手性等离激元超表面集成的复合结构示意图,左手性和右手性等离激元超表面的吸收光谱[43]

infrared detector. PMC structures manipulate photonic modes at a sub-wavelength scale to enhance the photoelectric coupling and increase the absorption of quantum wells[44]. The double polarization selection mechanism of the PMC and the quantum wells enhance the linear polarization extinction ratio up to 136 in the long wavelength infrared regime. Fig. 5 (a) shows the schematic diagram of the three-dimensional simulation of the plasma microcavity quantum well infrared detector and the reconstruction of the Stokes parameters.

In 2020, Chu et al. integrated asymmetric metamaterials on quantum wells for a long-wave infrared circular polarization detector. Based on the double polarization selection mechanism, a CPER of 14 is obtained[45]. This value is 10 times higher than that of the asymmetric metamaterial integrated HgCdTe detector. HgCdTe is the most widely used infrared detection material[46-47]. However, the CPER of the asymmetric metamaterial integrated HgCdTe detector is much lower since there is no double polarization selection. The double polarization selection mechanism is generally applicable to a variety of devices. When the asymmetric metamaterial is integrated with another anisotropic infrared detection material (InAsSb nanowire array), the CPER of this device is 12.6 in the mid-infrared region. In comparison, when the same asymmetric metamaterial is integrated into an InAsSb bulk material, the CPER is only 1.7. In addition, the integration of anisotropic optoelectronic materials and asymmetric metamaterials yields an improved CPER without compromising the absorptivity of active materials. High-intensity photonic modes excited by the asymmetric metamaterials can increase the absorption in the active materials by several times. Fig. 5 (b) shows the schematic composite structure of the asymmetric metamaterial and the detection material. and the absorption and reflection spectra of the anisotropic composite structure under left-handed circularly polarized light and right-handed circularly polarized light.

The bowtie antenna and aligned single-walled carbon nanotube (SWCNT) films integrated infrared detector, proposed by our research group, can be utilized for highly polarization-sensitive far-infrared detection, with a polarization extinction ratio exceeding 13 600 at a resonance frequency of 0.5 THz[48]. Our proposed plasmonic microcavity-integrated graphene photodetector for polarization detection achieves a polarization extinction ratio of approximately 30 at a wavelength of 1.55 μm[49-50]. In addition, the research group has also designed quantum well infrared photodetectors (QWIPs) integrated with all-semiconductor strip plasmonic cavities with high polarization sensitivity, and the polarization extinction ratio exceeds 900 in the terahertz band[51]. In the long-wave range, our proposed asymmetric metamaterial integrated quantum well (anisotropic material) has a CPER of approximately 14 [45]. This CPER is twice as high as that observed for graphene integrated with chiral plasmonic nanoantenna electrodes in the mid-infrared band[52].

2.3 Configurable photocurrent polarity by the optical structure

By integrating polarization-sensitive materials with micro-nano optical structures, high responsivity, and polarization extinction ratio has been achieved. Recently, configurable photocurrent polarity has also been realized by integrating plasmonic nanoantennas. The polarity of

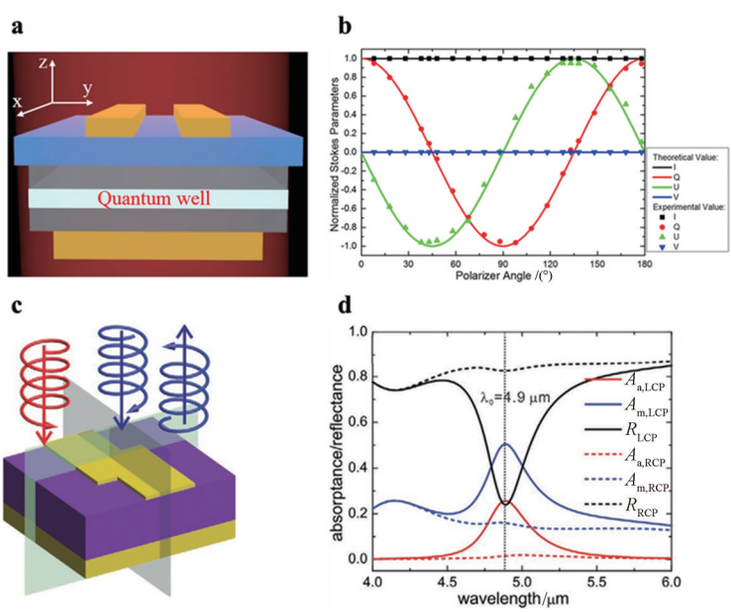

Fig. 5 (a) Schematic diagram of 3D simulation of plasmonic microcavity quantum well infrared detector, (b) Resolution of Stokes parameters[44], (c) Schematic diagram of the asymmetric composite structure, (d) Absorption and reflection spectra of anisotropic dielectric composite structures under LCP and RCP illumination[45]

图5 (a) 等离激元微腔集成的量子阱红外探测器的三维仿真示意图, (b) Stokes参数的解析[44], (c) 非对称复合结构示意图, (d) 左旋圆偏振和右旋圆偏振入射下, 各向异性介质复合结构的吸收和反射光谱[45]

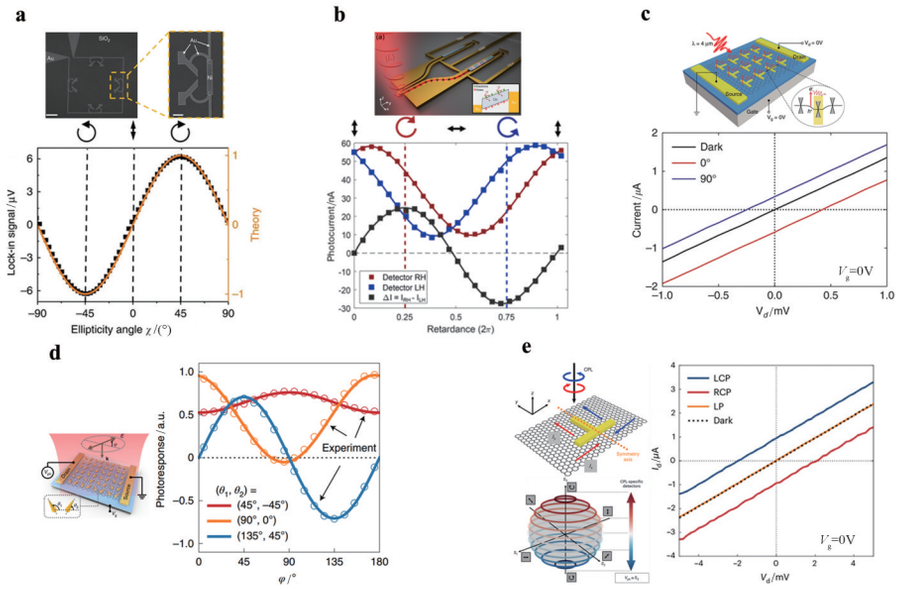

Fig. 6　(a) Scanning electron microscope image of a thermopile element. Measured thermoelectric reactor emf voltage (black dots) as a function of incident light ellipticity angle χ compared to normalized S_3 Stokes parameters at a wavelength of 7.9 μm and a light intensity of 270 W cm^{-2}[53]; (b) Device schematic for spin-controlled unidirectional plasmonic waveguide on-chip electrical detection. A Soleil-Babinet variable phase retarder was employed to convert linearly polarized laser radiation into left and right circular polarization states of intermediate elliptical and orthogonal linear polarization states[54]; (c) Schematic of a metasurface-mediated graphene photodetector. *I-V* curves of the device under dark and light conditions[55]; (d) Schematic of a nanoantenna-mediated semimetal photodetector. Measured (symbols) and fitted (dashed lines) photovoltage versus polarization angle for different gate voltages[56]; (e) Symmetry analysis of the photoresponse of an achiral plasmonic nanostructure located on a graphene sheet. Measured *I-V* curve with drain-source bias. Illustration of a CPL-specific photodetector in a Poincaré sphere, where the photovoltage V_{ph} depends only on the fourth Stokes parameter S_3 of the incident light[57]

图6　(a) 热电堆单元结构的扫描电子显微镜图像,在入射波长为7.9 μm,光强为270 W cm^{-2}时,实测随入射光椭圆率角χ变化的热电堆电动势电压值(黑点),及其与理论的归一化Stokes参数S_3分量的比较[53],(b) 自旋调控的单向等离激元波导片上电学探测器示意图,采用Soleil-Babinet可变相位延迟器将线偏光转换为椭圆偏振态、正交的线偏振态以及左旋和右旋圆偏振态[54],(c) 超表面调控的石墨烯光电探测器示意图,暗态和光照下的电流-电压曲线[55],(d) 纳米天线调控的半金属光电探测器示意图,不同栅电压下随偏振角变化的光电压,实测(圆圈符号)和拟合(虚线)[56],(e) 石墨烯薄片上非手性等离激元纳米结构光响应的对称性分析,不同源漏偏置下的电流-电压曲线,圆偏振光探测器在庞加莱球上的表示,其光电压只正比于入射光Stokes参数的S_3分量[57]

photocurrent can be tuned by light polarization flexibly and an infinite extinction ratio is realized at the polarity-transition point. In such cases, the traditional definition of polarization extinction ratio is no longer applicable, and the corresponding extinction ratio at the photocurrent polarity-transition approaches infinity.

In 2016, Lu et al. placed the thermal junction of a thermocouple at the center of an optical antenna to create an antenna-coupled thermopile photodetector[53]. The device is only sensitive to light ellipticity, and an antenna-coupled thermopile photodetector is used to convert the degree of circular polarization of light into a DC voltage proportional to the S_3 Stokes parameter of the incident radiation. The detector produces a bipolar voltage output that is proportional to the S_3 Stokes parameter of the incident light in the 7 ~ 9 μm wavelength range. The detector design is completely achiral, indicating that the incident light's chirality is converted into either the current direction or the DC voltage sign in the detector.

In 2019, Thomaschewski et al. combined strong light-matter interactions in plasmons with semiconductor technology based on spin-orbit interactions in achiral plasmonic nanocircuits[54]. They achieved this by integrating two gold-germanium-gold chiral plasmonic waveguide photodetectors, resulting in a compact polarimeter capable of detecting the circular polarization light.

In 2021, Wei et al. developed nanoantenna-mediated few-layer graphene photodetectors. The device allows for configurable switching between unipolar and bipolar polarization dependence of linear polarization response in the mid-infrared region through vectorial and nonlocal photoresponses[55-56]. The orientation of the nanoantenna in the device can be adjusted to vary the polarization extinction ratio from positive to negative, covering all possible values, with the polarization extinction ratio approaching infinity at the polarity-transition point. This

enables linearly polarized light detection with a range from finite to infinite extinction ratio.

Recently, in 2022, Wei et al. developed a mid-infrared circular polarization detection device by integrating plasmonic nanostructure arrays and graphene ribbons[57]. The geometric arrangement of plasmonic nanostructures enhances circularly polarized light detection, and the photocurrent generated by the achiral structure achieves a CPER of 84 under zero bias in the mid-infrared band at room temperature. The detection of CPL should be robust, with immunity against the ubiquitous unpolarized and linearly polarized light.

3 Challenge and opportunity: On-chip full-stokes detection

On-chip infrared polarization detection has been extensively studied nowadays. The perception of a single polarization state has been thoroughly studied. Full Stokes detection that includes all polarization information becomes a challenge and opportunity.

In 2020, Li et al. developed four metasurface-integrated graphene-silicon photodetectors based on the geometric chirality and anisotropy of the metasurface for circular and linear polarization-resolved light responses[58]. The photodetector enables full Stokes parameter detection for arbitrary polarized incident infrared light at 1 550 nm.

In 2021, Zhou et al. coupled four single-mode silicon waveguides to a circle-like polarization distinguishing device on an insulating silicon substrate to create an on-chip optical polarimeter capable of measuring arbitrary polarization states[59].

In 2022, Xiong et al. developed a fiber-integrated polarimeter by vertically stacking three photodetection units based on two-dimensional vdW materials on the fiber end face[60]. The polarimeter consists of six layers of van der Waals materials stacked vertically to form three photodetection units. Two anisotropic BP units are twisted stacked for polarized light sensing, and a bismuth selenide (Bi_2Se_3) layer provides power calibration. The polarimeter features self-power-calibration, self-driven, and ambiguity-free detection of linearly and circularly polarized light by breaking symmetry-induced LPGEs and

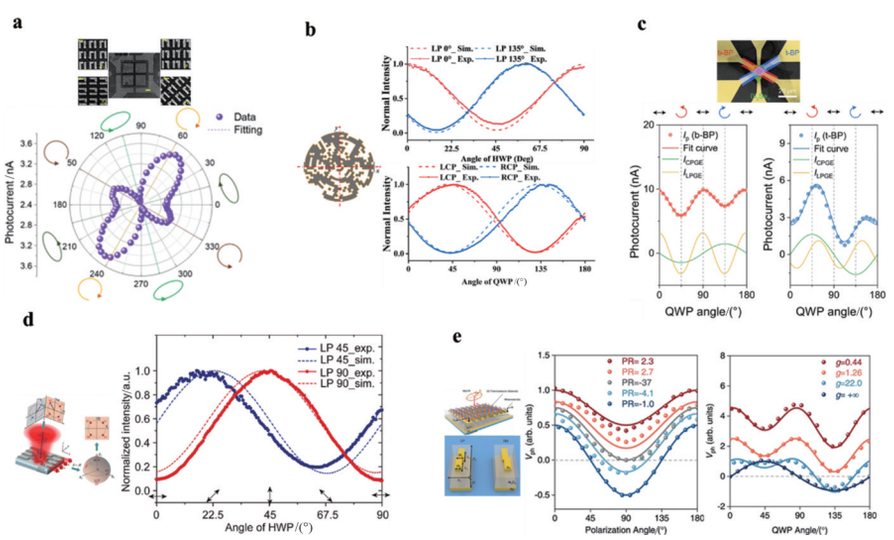

Fig. 7 (a) SEM image of a polarimeter. Polar plot of photoresponse as a function of quarter-wave plate (QWP) rotation angle[58]; (b) SEM image of the device. Simulations and experiments examine the intensity of the 0° and 135° linearly polarized light (LP) components as a function of the half-wave plate (HWP). Simulations and experiments examine the intensity of different QWP angles for left-handed circularly polarized light (LCP) and right-handed circularly polarized light (RCP) components[59]; (c) False-color SEM image of a fiber end-face stack. One cycle photocurrent of the twisted BP cell as a function of QWP angle[60]; (d) Schematic diagram of on-chip phase demodulation for high-speed coherent optical communication. The normalized output intensities of different waveguide ports for a single nanodisk element and two double nanodisk elements were experimentally measured and simulated[61]; (e) Structural design of resonant thermoelectric photoresponse. Polarization-angle-dependent photoresponse simulations (lines) and measurements (symbols) for five typical devices. Simulated (line) and measured (symbol) photoresponses of four typical devices as a function of QWP angle[62]

图7 (a) 偏振计的扫描电子显微镜图像,随四分之一波片角度变化的光响应[58],(b) 器件的扫描电子显微镜图像,仿真和实测的0°和135°线偏振分量随二分之一波片角度变化的强度,以及左旋和右旋圆偏振分量随四分之一波片角度变化的强度[59],(c) 光纤端面堆叠结构的伪彩色扫描电子显微镜图像,扭曲黑磷单元结构随四分之一波片角度变化的光电流[60],(d) 高速相干光通信中,片上相位解调的示意图,对于单个纳米盘和两个双纳米盘,实测和仿真的不同波导端口输出的归一化强度[61],(e) 共振热电光响应的器件结构设计示意图,5个典型器件不同的随偏振角变化的光响应,仿真(实线)和实测(圆形符号),4种典型器件不同的随四分之一波片角度变化的光响应,仿真(实线)和实测(圆形符号)[62]

CPGEs in the two BP units.

In 2022, Lei et al. coupled a network of single-mode Si waveguides to an insulating silicon substrate to achieve on-chip high-speed coherent optical signal detection based on photon spin-orbit interactions and enable full Stokes parameter measurement of incident light[61].

In 2022, Dai et al. integrated plasmonic chiral materials and two-dimensional thermoelectric materials to prepare an on-chip mid-infrared photodetector[62]. The photodetector is based on the polarization-dependent photothermal effect in chiral plasmonic metamaterial-mediated and the Seebeck effect of two-dimensional thermoelectric materials. It enables the detection of linearly polarized and circularly polarized light and realizes on-chip full Stokes detection in the mid-infrared band at room temperature. However, the average measurement errors are large. The error of S_1, S_2, and S_3 are 14.2%, 15.2%, and 5.4%, respectively. More accurate on-chip full-Stokes detection is desired.

4 Conclusion

Many different approaches and significant efforts have been dedicated to the advances of on-chip infrared polarization detectors. These polarization detectors can be realized by polarization-sensitive materials including anisotropic two-dimensional materials, topological materials, chiral materials, and integrated polarization-selective optical coupling structures. When polarization-selective optical coupling structures and polarization selective detection materials are combined in a proper way, high polarization discrimination can be achieved. With the development of artificial metamaterials-mediated detectors, the polarity of photocurrent can be flexibly tuned by light polarization, and an infinite extinction ratio could be realized at the polarity-transition point. In conclusion, on-chip polarization detection by integrating anisotropic materials and optical structure has received widespread attention. In the future, on-chip full Stokes parameters detection with high accuracy of all polarization states covering the full Poincare sphere presents challenges and opportunities.

References

[1] Tyo J S, Goldstein D L, Chenault D B, *et al*. Review of passive imaging polarimetry for remote sensing applications [J]. *Applied Optics*, 2006, **45**(22): 5453.

[2] Li L, Han W, Pi L, *et al*. Emerging in-plane anisotropic two-dimensional materials[J]. *InfoMat*, 2019, **1**(1): 54-73.

[3] Wang Y, Wu P, Wang Z, *et al*. Air-stable low-symmetry narrow-bandgap 2D sulfide niobium for polarization photodetection [J]. *Advanced Materials*, 2020, **32**(45): 2005037.

[4] Beddiar M I, Zhang X, Liu B, *et al*. Ambipolar-to-unipolar conversion in ultrathin 2D semiconductors [J]. *Small Structures*, 2022, **3**(12): 2200125.

[5] Buscema M, Groenendijk D J, Blanter S I, *et al*. Fast and broadband photoresponse of few-layer black phosphorus field-effect transistors[J]. *Nano Letters*, 2014, **14**(6): 3347-3352.

[6] Liu Y, Sun T, Ma W, *et al*. Highly responsive broadband black phosphorus photodetectors[J]. *Chinese Optics Letters*, 2018, **16**(2): 020002.

[7] Perello D J, Chae S H, Song S, *et al*. High-performance n-type black phosphorus transistors with type control via thickness and contact-metal engineering [J]. *Nature Communications*, 2015, **6**(1): 7809.

[8] Mao N, Tang J, Xie L, *et al*. Optical anisotropy of black phosphorus in the visible regime [J]. *Journal of the American Chemical Society*, 2016, **138**(1): 300-305.

[9] Han F W, Zhao C X, Zhang Y M. Photoelectric properties of monolayer black phosphorus in visible regime at room temperature [J]. *AIP Advances*, 2019, **9**(5): 055216.

[10] Hong T, Chamlagain B, Lin W, *et al*. Polarized photocurrent response in black phosphorus field-effect transistors [J]. *Nanoscale*, 2014, **6**(15): 8978-8983.

[11] Chen X, Lu X, Deng B, *et al*. Widely tunable black phosphorus mid-infrared photodetector [J]. *Nature Communications*, 2017, **8**(1): 1672.

[12] Akamatsu T, Ideue T, Zhou L, *et al*. A van der Waals interface that creates in-plane polarization and a spontaneous photovoltaic effect [J]. *Science*, 2021, **372**(6537): 68-72.

[13] Deng Y, Luo Z, Conrad N J, *et al*. Black phosphorus-monolayer MoS2 van der waals heterojunction p-n diode[J]. *ACS Nano*, 2014, **8**(8): 8292-8299.

[14] Chen P, Xiang J, Yu H, *et al*. Gate tunable MoS2 - black phosphorus heterojunction devices[J]. *2D Materials*, 2015, **2**(3): 034009.

[15] Jiang X, Zhang M, Liu L, *et al*. Multifunctional black phosphorus/MoS2 van der Waals heterojunction [J]. *Nanophotonics*, 2020, **9**(8): 2487-2493.

[16] Hu T, Zhang R, Li J-P, *et al*. Photodetectors based on two-dimensional MoS2 and its assembled heterostructures [J]. *Chip*, 2022, **1**(3): 100017.

[17] Bullock J, Amani M, Cho J, *et al*. Polarization-resolved black phosphorus/molybdenum disulfide mid-wave infrared photodiodes with high detectivity at room temperature[J]. *Nature Photonics*, 2018, **12**(10): 601-607.

[18] Rasmita A, Jiang C, Jiang C, *et al*. Tunable geometric photocurrent in van der Waals heterostructure [J]. *Optica*, 2020, **7**(9): 1204-1208.

[19] Chen Y, Wang Y, Wang Z, *et al*. Unipolar barrier photodetectors based on van der Waals heterostructures [J]. *Nature Electronics*, 2021, **4**(5): 357-363.

[20] Wu P, Ye L, Tong L, *et al*. Van der Waals two-color infrared photodetector[J]. *Light: Science & Applications*, 2022, **11**(1): 6.

[21] Chen C, Lu X, Deng B, *et al*. Widely tunable mid-infrared light emission in thin-film black phosphorus[J]. *Science Advances*, 2020, **6**(7): eaay6134.

[22] Lai J, Liu X, Ma J, *et al*. Anisotropic broadband photoresponse of layered type-II weyl semimetal $MoTe_2$ [J]. *Advanced Materials*, 2018, **30**(22): 1707152.

[23] Ma J, Cheng B, Li L, *et al*. Unveiling Weyl-related optical responses in semiconducting tellurium by mid-infrared circular photogalvanic effect[J]. *Nature Communications*, 2022, **13**(1): 1-7.

[24] Wang R, Li L, Tian H, *et al*. Full telecomband covered half-wave meta-reflectarray for efficient circular polarization conversion [J]. *Optics Communications*, 2018, **427**: 469-476.

[25] Zhou J, Deng J, Shi M, *et al*. Cavity coupled plasmonic resonator enhanced infrared detectors [J]. *Applied Physics Letters*, 2021, **119**(16): 160504.

[26] Jiang F, Shi M, Zhou J, *et al*. Integrated photonic structure enhanced infrared photodetectors [J]. *Advanced Photonics Research*, 2021, **2**(9): 2000187.

[27] Chen W, Zhao Z, Wang C, *et al*. Linear polarization grating combining a circular polarization grating with a special cycloidal diffractive quarter waveplate[J]. *Optics Express*, 2019, **27**(23): 33378-33390.

[28] Zhou R, Ullah K, Yang S, *et al*. Recent advances in graphene and black phosphorus nonlinear plasmonics[J]. *Nanophotonics*, 2020, **9**(7): 1695-1715.

[29] Tong L, Huang X, Wang P, *et al*. Stable mid-infrared polarization imaging based on quasi-2D tellurium at room temperature [J]. *Nature Communications*, 2020, **11**(1): 2308.

[30] Deng W, Dai M, Wang C, *et al*. Switchable unipolar-barrier van der waals heterostructures with natural anisotropy for full linear polarimetry detection[J]. *Advanced Materials*, 2022, **34**(33): 2203766.

[31] Fang C, Li J, Zhou B, *et al*. Self-Powered Filterless On-Chip Full-Stokes Polarimeter[J]. *Nano Letters*, 2021, **21**(14): 6156-6162.

[32] Ma C, Yuan S, Cheung P, *et al*. Intelligent infrared sensing enabled by tunable moiré quantum geometry[J]. *Nature*, 2022, **604**(7905): 266-272.

[33] Xu S-Y, Ma Q, Shen H, *et al*. Electrically switchable Berry curvature dipole in the monolayer topological insulator WTe_2 [J]. *Nature*

Physics, 2018, **14**(9): 900-906.
[34] Osterhoudt G B, Diebel L K, Gray M J, *et al*. Colossal mid-infrared bulk photovoltaic effect in a type-I Weyl semimetal[J]. *Nature Materials*, 2019, **18**(5): 471-475.
[35] Zhang C, Wang X, Qiu L. Circularly Polarized Photodetectors Based on Chiral Materials: A Review[J]. *Frontiers in Chemistry*, 2021, **9**: 711488.
[36] Chen C, Gao L, Gao W, *et al*. Circularly polarized light detection using chiral hybrid perovskite[J]. *Nature Communications*, 2019, **10**(1): 1927.
[37] Ishii A, Miyasaka T. Direct detection of circular polarized light in helical 1D perovskite-based photodiode[J]. *Science Advances*, 2020, **6**(46): eabd3274.
[38] Liu Z, Zhang C, Liu X, *et al*. Chiral Hybrid Perovskite Single-Crystal Nanowire Arrays for High-Performance Circularly Polarized Light Detection[J]. *Advanced Science*, 2021, **8**(21): 2102065.
[39] Cao Y, Li C, Deng J, *et al*. Enhanced photodetector performance of black phosphorus by interfacing with chiral perovskite[J]. *Nano Research*, 2022, **15**(8): 7492-7497.
[40] Li Q, Li Z, Li N, *et al*. High-Polarization-Discriminating Infrared Detection Using a Single Quantum Well Sandwiched in Plasmonic Micro-Cavity[J]. *Scientific Reports*, 2015, **4**(1): 6332.
[41] Li W, Coppens Z J, Besteiro L V, *et al*. Circularly polarized light detection with hot electrons in chiral plasmonic metamaterials[J]. *Nature Communications*, 2015, **6**(1): 8379.
[42] Wang M, Salut R, Lu H, *et al*. Subwavelength polarization optics via individual and coupled helical traveling-wave nanoantennas [J]. *Light: Science & Applications*, 2019, **8**(1): 76.
[43] Jiang Q, Du B, Jiang M, *et al*. Ultrathin circular polarimeter based on chiral plasmonic metasurface and monolayer $MoSe_2$ [J]. *Nanoscale*, 2020, **12**(10): 5906-5913.
[44] Zhou Y W, Li Z F, Zhou J, *et al*. High extinction ratio super pixel for long wavelength infrared polarization imaging detection based on plasmonic microcavity quantum well infrared photodetectors[J]. *Scientific Reports*, 2018, **8**(1): 15070.
[45] Chu Z, Zhou J, Dai X, *et al*. Circular polarization discrimination enhanced by anisotropic media[J]. *Advanced Optical Materials*, 2020, **8**(9): 1901800.
[46] Hu W, Ye Z, Liao L, *et al*. 128 × 128 long-wavelength/mid-wavelength two-color HgCdTe infrared focal plane array detector with ultralow spectral cross talk[J]. *Optics Letters*, 2014, **39**(17): 5184-5187.
[47] Hu W D, Chen X S, Ye Z H, *et al*. A hybrid surface passivation on HgCdTe long wave infrared detector with in-situ CdTe deposition and high-density hydrogen plasma modification[J]. *Applied Physics Letters*, 2011, **99**(9): 091101.
[48] Chen B, Ji Z, Zhou J, *et al*. Highly polarization-sensitive far infrared detector based on an optical antenna integrated aligned carbon nanotube film[J]. *Nanoscale*, 2020, **12**(22): 11808-11817.
[49] Guo S, Zhang D, Zhou J, *et al*. Enhanced infrared photoresponse induced by symmetry breaking in a hybrid structure of graphene and plasmonic nanocavities[J]. *Carbon*, 2020, **170**: 49-58.
[50] Zhang D, Zhou J, Liu C, *et al*. Enhanced polarization sensitivity by plasmonic-cavity in graphene phototransistors[J]. *Journal of Applied Physics*, 2019, **126**(7): 074301.
[51] Deng J, Zheng Y, Zhou J, *et al*. Absorption enhancement in all-semiconductor plasmonic cavity integrated THz quantum well infrared photodetectors[J]. *Optics Express*, 2020, **28**(11): 16427.
[52] Peng J, Cumming B P, Gu M. Direct detection of photon spin angular momentum by a chiral graphene mid-infrared photodetector[J]. *Optics Letters*, 2019, **44**(12): 2998.
[53] Lu F, Lee J, Jiang A, *et al*. Thermopile detector of light ellipticity [J]. *Nature Communications*, 2016, **7**(1): 12994.
[54] Thomaschewski M, Yang Y, Wolff C, *et al*. On-chip detection of optical spin-orbit interactions in plasmonic nanocircuits[J]. *Nano Letters*, 2019, **19**(2): 1166-1171.
[55] Wei J, Li Y, Wang L, *et al*. Zero-bias mid-infrared graphene photodetectors with bulk photoresponse and calibration-free polarization detection[J]. *Nature Communications*, 2020, **11**(1): 6404.
[56] Wei J, Xu C, Dong B, *et al*. Mid-infrared semimetal polarization detectors with configurable polarity transition [J]. *Nature Photonics*, 2021, **15**(8): 614-621.
[57] Wei J, Chen Y, Li Y, *et al*. Geometric filterless photodetectors for mid-infrared spin light[J]. *Nature Photonics*, 2022, **17**: 171-178.
[58] Li L, Wang J, Kang L, *et al*. Monolithic full-stokes near-infrared polarimetry with chiral plasmonic metasurface integrated graphene-silicon photodetector[J]. *ACS Nano*, 2020, **14**(12): 16634-16642.
[59] Zhou C, Xie Y, Ren J, *et al*. Spin separation based on-chip optical polarimeter via inverse design [J]. *Nanophotonics*, 2022, **11**(4): 813-819.
[60] Xiong Y, Wang Y, Zhu R, *et al*. Twisted black phosphorus-based van der Waals stacks for fiber-integrated polarimeters [J]. *Science Advances*, 2022, **8**(18): eabo0375.
[61] Lei T, Zhou C, Wang D, *et al*. On-chip high-speed coherent optical signal detection based on photonic spin-hall effect[J]. *Laser & Photonics Reviews*, 2022, **16**(9): 2100669.
[62] Dai M, Wang C, Qiang B, *et al*. On-chip mid-infrared photothermoelectric detectors for full-Stokes detection [J]. *Nature Communications*, 2022, **13**(1): 4560.